Carbon 129 (2018) 8–14

Contents lists available at ScienceDirect

Carbon

journal homepage: www.elsevier.com/locate/carbon

Modulation of the effective density and refractive index of carbon nanotube forests via nanoimprint lithography

Sei Jin Park [a, b, *, 1], Jong G. Ok [b, c, d, **, 1], Hui Joon Park [c, e], Kyu-Tae Lee [c, f], Jae Hyuk Lee [d], Jeong Dae Kim [d], Eikhyun Cho [g], Hyoung Won Baac [c, h], Shinill Kang [g], L. Jay Guo [c, ***], A. John Hart [a, b, ****]

[a] Department of Mechanical Engineering, Massachusetts Institute of Technology, Cambridge, MA 02139, USA
[b] Department of Mechanical Engineering, University of Michigan, Ann Arbor, MI 48109, USA
[c] Department of Electrical Engineering, University of Michigan, Ann Arbor, MI 48109, USA
[d] Department of Mechanical and Automotive Engineering, Seoul National University of Science and Technology, Seoul 01811, South Korea
[e] Department of Electrical and Computer Engineering, Department of Energy Systems Research, Ajou University, Suwon 16499, South Korea
[f] Department of Materials Science and Engineering, University of Illinois at Urbana-Champaign, Urbana, IL 61801, USA
[g] School of Mechanical Engineering, Yonsei University, Seoul 03722, South Korea
[h] School of Electronic and Electrical Engineering, Sungkyunkwan University, Suwon 16419, South Korea

ARTICLE INFO

Article history:
Received 4 August 2017
Received in revised form
22 November 2017
Accepted 25 November 2017
Available online 1 December 2017

ABSTRACT

The unique properties of carbon nanotubes (CNTs) allow them to be used in various optical applications, such as ultra-dark surfaces, bolometers, metamaterial cloaks, and anisotropic absorbers. In particular, organization of CNTs with controlled density at the sub-micrometer scale could enable new strategies to engineer optically active surfaces. Here, we present a new strategy to engineer the density-dependent optical properties of CNT forests by patterning of catalyst film via nanoimprint lithography (NIL) followed by atmospheric pressure chemical vapor deposition (CVD) synthesis of CNTs. Via this approach, we demonstrate atmospheric pressure growth of CNT structures with widths of 80–350 nm. These structures form self-supporting arrays with height exceeding 500 μm, representing aspect ratios well over 1000:1. Optical attenuation measurement places the density of NIL patterned forests to be a fraction of the density of unpatterned CNT forests, confirming that the CNT density is effectively controlled by the catalyst coverage. The infrared absorbance measurements corroborate the density control, and Kramers-Kronig analysis shows that the refractive indices of the NIL patterned CNT forests are tunable in the range of 1–1.8.

1. Introduction

Carbon nanotubes (CNTs [1–5]) in various micro- and macro-scale forms have been widely studied as thermal and electrical interface materials [6,7], electronic devices [8–11], and mechanical metamaterials [12]. In addition, due to their highly anisotropic nanoscale filamentary structure, CNTs can be configured for optical applications such as ultra-dark surfaces [13,14], bolometers [15], cloaks [16,17], waveguides [18] and anisotropic absorbers [19]. For instance, ultra-dark surfaces are useful for preventing stray light from entering sensitive optics, and engineered absorbers can improve the sensitivity of radiometric devices. For these applications, scalable methods to control CNT density are necessary to enable further engineering of optical properties.

One prominent method of forming CNT-based surfaces for optical applications is by chemical vapor deposition (CVD) of vertically aligned CNT "forests". Modulation of the CNT density within the forest is one means of influencing its surface and bulk optical properties. Previously reported attempts to control the CNT density

* Corresponding author. Department of Mechanical Engineering, Massachusetts Institute of Technology, Cambridge, MA 02139, USA.
** Corresponding author. Department of Mechanical and Automotive Engineering, Seoul National University of Science and Technology, Seoul 01811, South Korea.
*** Corresponding author. Department of Mechanical Engineering, University of Michigan, Ann Arbor, MI 48109, USA.
**** Corresponding author. Department of Mechanical Engineering, Massachusetts Institute of Technology, Cambridge, MA 02139, USA.
E-mail addresses: psj@mit.edu (S.J. Park), jgok@seoultech.ac.kr (J.G. Ok), guo@umich.edu (L.J. Guo), ajhart@mit.edu (A.J. Hart).
[1] These authors contributed equally to this work.

https://doi.org/10.1016/j.carbon.2017.11.079
0008-6223/

are either based on tuning the catalytic site density or the growth condo. Examples of the former approach include placing catalyst particles via pulse-current electrochemical deposition [20] and block co-polymer film casting [21–25], or by modifying the catalyst film de-wetting via changing the catalyst/underlayer thicknesses [26,27], the grain size [28], or the precursor solution concentration [29]. The latter approach was demonstrated by changing catalyst pretreatment [30], hydrogen concentration [31], or the growth temperature [32]. While effective, these methods typically produce randomly tangled CNT films, and in the cases that the CNTs are sufficiently dense to be vertically aligned or thick enough to stand vertically alone, either their lengths were limited to a few tens of microns at most, or the resulting forests were highly dense (>50 kg/m^3) [31].

Here we demonstrate a new approach to modulating the effective density of CNTs in macroscale films, by sub-micrometer patterning of the CNT growth catalyst using nanoimprint lithography (NIL). We show that NIL can be employed to create catalyst films having 1D and 2D grating patterns with well-controlled sub-micrometer dimensions. CNT forests grown from these patterns have periodic nanotextures matching the imprinted patterns, thus varying the effective CNT density and the resulting refractive index. This texture based density tuning enables growth of thick (~100s of microns) vertically aligned CNT films with prescribed anisotropic optical properties, contrasting randomly tangled mats [33] or horizontally aligned CNT films [19] used for optical applications.

2. Experimental section

2.1. Nanoimprint patterning of CNT catalyst

CNT catalyst was patterned by nanoimprint lithography (NIL) as schematically shown in Fig. 1a. First, a polymer resin (MRI-8020,

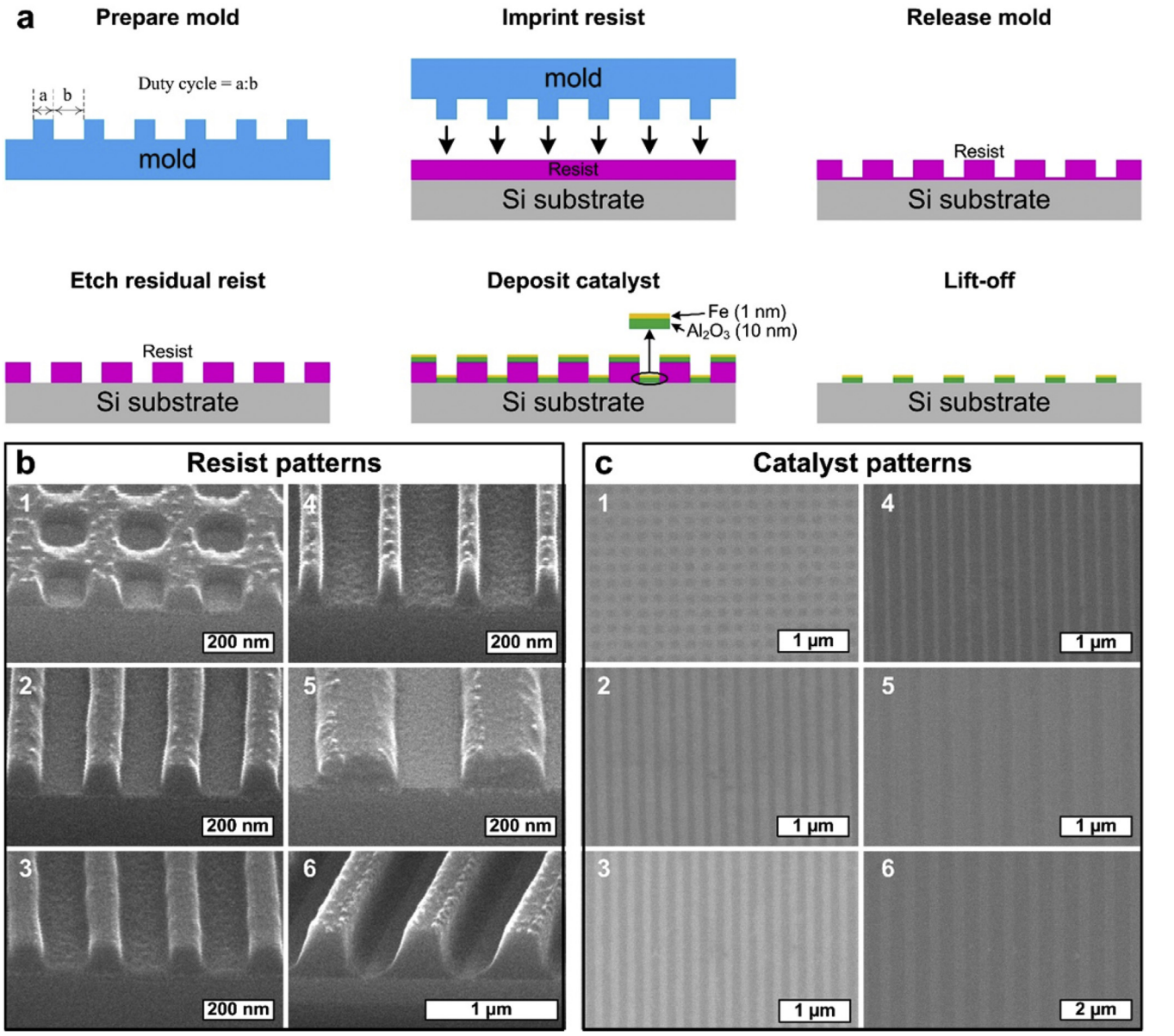

Fig. 1. a) Steps of nanoimprint lithography process used to pattern CNT growth catalyst. b) SEM images showing the resist structures after the imprint and etching steps. c) SEM images showing the corresponding patterned CNT catalyst after lift-off. The feature dimensions range from 70 to 700 nm. (A colour version of this figure can be viewed online.)

Microresist Technology GmbH) was spin-coated on a cleaned SiO_2/Si substrate and imprinted by a rigid mold containing the inverse profile of the desired pattern. The detailed NIL processing conditions along with mold fabrication procedure can be found elsewhere [34]. The residual layer of imprinted resin was removed by reactive ion etching using O_2 plasma (LAM 9400 SE, LAM Research Corporation). Then, the 10 nm of alumina followed by 1 nm of Fe are sputtered (Lab 18, Kurt J. Lesker) on the patterned substrates to create catalyst stacks needed for CNT growth. The prepared substrates were subsequently diced using a die saw into 10 mm by 1 mm pieces for density measurement following the growth of CNTs on them. Lift-off was performed by ultrasonication in acetone and rinsing with isopropanol then blow-drying with dry air.

2.2. CNT growth

A thermal CVD system was used to perform CNT growth. The system comprises a temperature controlled tube furnace with a 25 mm diameter quartz tube, and electronic mass flow controllers (MFCs; Aalborg). The NIL-patterned CNT catalyst substrates are placed on a quartz platform that measures 75 mm by 18 mm, which is connected to a magnetically coupled transfer arm adjacent to the quartz tube. Then the quartz tube is sealed, and a LabVIEW™ program is used to coordinate the gas flows ($He/H_2/C_2H_4$) and time-temperature sequence. The samples shown in this paper were produced by decoupling the catalyst annealing and CNT growth steps using rapid insertion and withdrawal of the sample from the furnace (the 'decoupled recipe'), as described by *Li* et al. [35] For all experiments the CVD temperature was 775 °C and the growth duration was 5 min.

2.3. Optical characterization

The mass density of CNT forests was characterized by measuring the optical attenuation of a 633 nm laser passing through the forest [36], relative to a mass density-optical attenuation relationship of unpatterned CNT forests. The density-attenuation relationship was obtained by growing unpatterned CNT forests on 10 × 1 mm silicon substrates. The optical attenuation of a series of samples was recorded, and the mass of the CNT forests were measured using a microbalance after removing the CNTs from the silicon substrates using a razor blade. All measurements were performed at the midpoint of the CNT forest side wall.

The specular reflectance of the CNT sample was measured in grazing incidence (ATR mode, 4 cm^{-1} resolution, 32 scans, 4000–400 cm^{-1} range) using a Fourier transform infrared (FT-IR) spectrometer (Vertex 70, Bruker). Complex refractive indices of the CNT samples were obtained by Kramers-Kronig constrained variational analysis of the measured reflectance spectra [37].

3. Results and discussion

Nanoimprint patterning of the CNT catalyst film is demonstrated using master molds with 1D (line) or 2D (dot) patterns spanning a range of coverage density and sub-micrometer lateral dimensions. Patterns used in this work are listed in Table S1, along with the corresponding final catalyst coverage on the substrate (referred to as the duty cycle). In Fig. 1b, we show photoresist structures after the imprint and etching steps, indicating that nanoscale patterns have been successfully formed with high fidelity. Following the catalyst deposition and subsequent lift-off steps, the patterned catalyst layer can be observed via scanning electron microscopy (SEM) due to the contrast between Fe and Al_2O_3 layers. The catalyst patterns are well defined over millimeter-scale areas, showing successful application of NIL.

After CNT growth by CVD for 5 min (see Methods), CNT forests with approximately 500 μm in height are observed (Fig. S1). Compared to the smooth sidewall of a non-patterned forest, SEM imaging (Fig. 2) reveals that the top and side walls of the forests grown from nanoimprinted catalyst have periodic textures matching the imprinted patterns. The patterns are clearly visible in the top view of the forest grown, despite some waviness and wrinkling, while the sidewalls of the NIL-patterned forests appear nearly homogeneous. This may be expected because the intrinsic waviness of the CNTs during growth causes the individual patterns to blend; the pattern spacing is on the same order as the CNT-CNT spacing (~100 nm) expected in similar CNT forests grown without patterning [38]. For example, with a pattern comprising squares (dots) with 110 nm side length (Fig. 2c), the individual pillars can be seen at the top of the surface, but it is hard to distinguish individual pillars from the side view. While the CNTs at the top of the pillars are bound into a tangled 'crust', the CNTs beneath are free from this constraint, and are free to bend away from each other to fill in the empty spaces. Line patterns (Fig. 2b) have clearer sidewall definition due to the greater mechanical constraint provided by the pattern design.

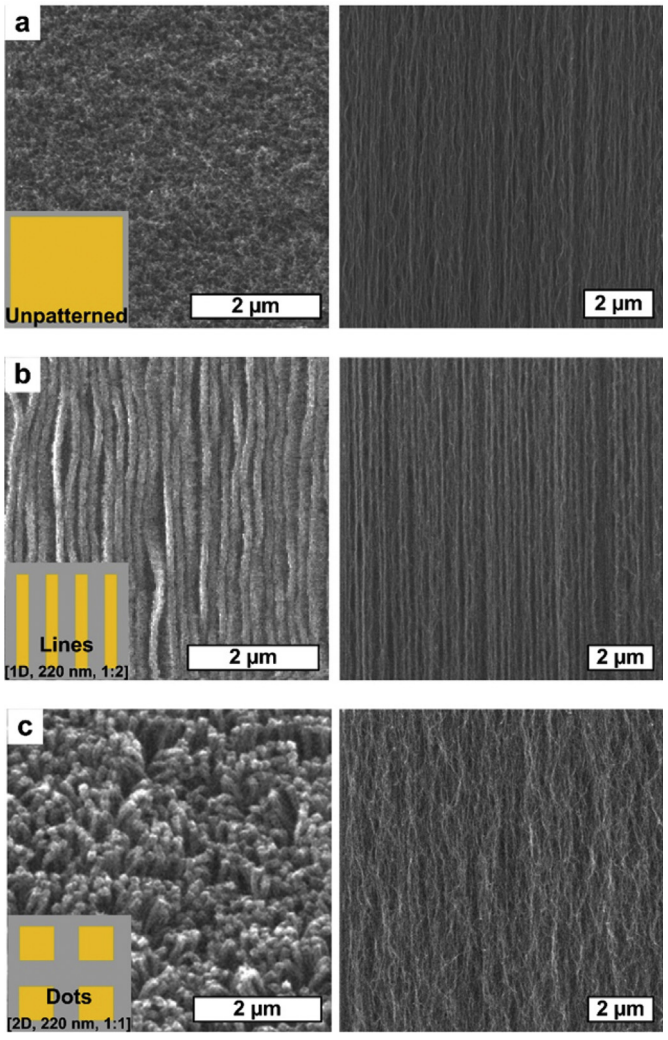

Fig. 2. SEM images showing sub-micrometer features of top (left) and side (right) surfaces of CNT forests grown from catalyst that is a) unpatterned, b) lines [1D, 220 nm, 1:2], and c) dots [2D, 220 nm, 1:1]. (A colour version of this figure can be viewed online.)

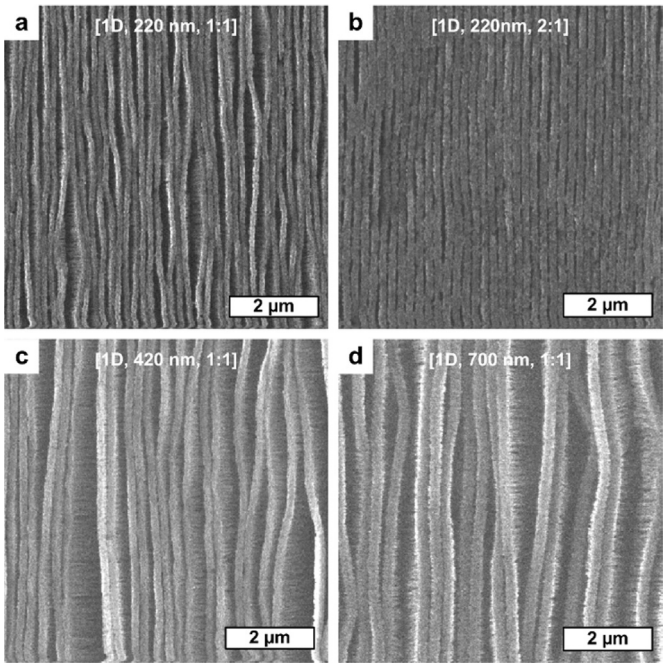

Fig. 3. SEM images showing top surfaces of CNT forests grown from NIL lines patterns, with a) [1D, 220 nm, 1:1], b) [1D, 220 nm, 2:1], c) [1D, 420 nm, 1:1], and d) [1D, 700 nm, 1:1].

In Fig. 3, we show a series of line patterns with [1D, 220 nm, 1:1], [1D, 220 nm, 2:1], [1D, 420 nm, 1:1], and [1D, 700 nm, 1:1]. In all cases the pattern shapes are well preserved through the film thickness (Fig. S2). Also, when the period is kept the same, thicker CNT lines are less wrinkled, presumably due their greater rigidity which counteracts the forces exerted by the growing CNTs [39]. Notably, the aspect ratio of the individual CNT nanostructures within the NIL-patterned forests easily exceeds ~5000:1, while isolated micropillars rarely exceed the aspect ratio of 10 without significant bending [40], showing that the mechanical constraint provided by periodic patterns is critical to prolonged vertical growth.

Because the NIL-patterned catalysts result in CNT forests with uniform texture on a length scale smaller than visible light, the influence of the pattern on effective density can be assessed using optical attenuation. Moreover, the average density of the CNT forest can be derived by treating the CNT forest to be an effective medium of individual absorbers. Therefore, as previously shown [36], the Beer-Lambert law can be used to calculate the average density of the NIL-patterned CNT forests as:

$$\mathrm{T} = \frac{I}{I_o} = e^{-\mu l}$$

where T is the transmittance which is a ratio of the intensity of transmitted light (I) over intensity of the incident light (I_o), μ is the attenuation coefficient, and l is the path length. Using identical samples, the path length is fixed in the above equation, and hence the optical depth (τ), which is the product of μ and l, can represent each sample's optical attenuation.

To provide a reference measure of mass density, a series of unpatterned forests was grown and their average volumetric mass densities were calculated using a microbalance and SEM measurements. Then, the optical depths were measured (see Methods) and a reference optical depth-mass density relationship was plotted (Fig. 4a). The relationship shows a nonlinear increase in

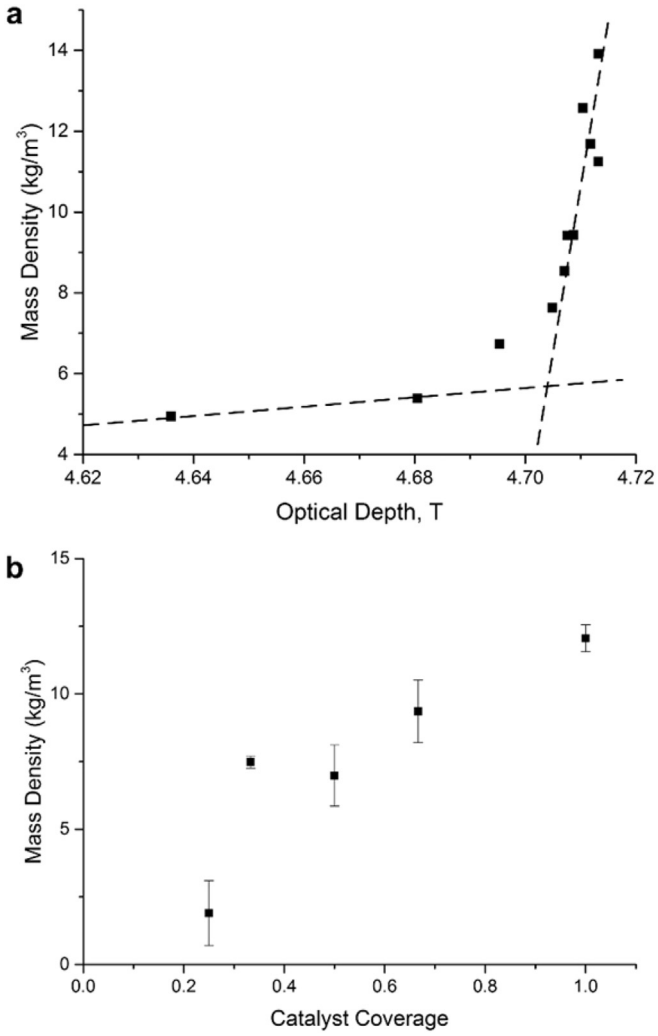

Fig. 4. a) Relationship between mass density and optical depth of unpatterned CNT forest, used as a reference to deduce NIL-CNT forest density. Two straight lines at the lower and higher optical depth values were used to estimate density of NIL-CNT forests whose measured optical depths fall beyond the range of the reference plot. b) Mass density of NIL-CNT forests plotted versus the catalyst coverage.

mass density as the optical depth increases, consistent with previous results [36], which shows initial linear relationship, and nonlinearity arising at higher optical depth.

Then, the optical depths of the NIL-patterned CNT samples were measured and their mass densities were deduced from the previously established relation (Fig. 4b). Note that two straight lines were used to estimate the mass density values at lower and higher ends of the optical depth axis, which are also shown in Fig. 4a. The catalyst coverage is a measure of how much area was covered with catalyst over the entire sample cross section, and was calculated based on SEM measurements of the pattern and spacing widths. This value for the unpatterned CNT forests would be 1, and it is evident that NIL patterned CNT forests only have a fraction of density of the unpatterned forest, as shown in Fig. 4b.

At a first glance, it seems that the mass density would scale linearly with the catalyst coverage with the intercept at the origin, as no catalyst coverage would mean no CNT growth. In reality, this relationship is shown to be sub-linear possibly because as the individual catalyst pattern dimensions approach average spacing between individual CNTs [38], the random catalyst film de-wetting may yield less than expected number of CNT nucleation sites, and/

or the concentration of chemical species produced by catalyst patches needed for growth of CNTs may shift, causing changes in the CNT population produced. Even at these small catalyst feature sizes, the chemical coupling between catalyst particles [41] results in uniform growth of CNTs across the patterned area. However, while the growth was uniform the low mass density implies that this is close to the lower limit of the catalyst coverage required to produce vertically aligned CNTs.

To assess the optical property tuning afforded by density control, we have performed FT-IR measurements of the NIL patterned CNT forests to obtain their refractive indices. The measured optical absorbance of the forests in grazing incidence (Fig. 5a) shows characteristic peaks expected from CNTs, including signatures of common functional groups adsorbed and/or bonded to CNTs from CVD synthesis, such as CH_x and −COOH. The IR absorption spectra of CNT forests depend on CNT characteristics, such as diameter, length, chirality and bundling [42,43] as well as the functional groups attached to the CNTs [44]. Especially, the IR modes of CNT population overlap in the energy window between 700 and 1300 cm^{-1} [42], and it can be seen that the intensity across peaks within this window is generally proportional to the pattern density. Similar IR modes in the range of 700–1300 cm^{-1} suggests that the CNTs that make up of the forests did not significantly change by the NIL patterning, except perhaps in the case of the lowest density.

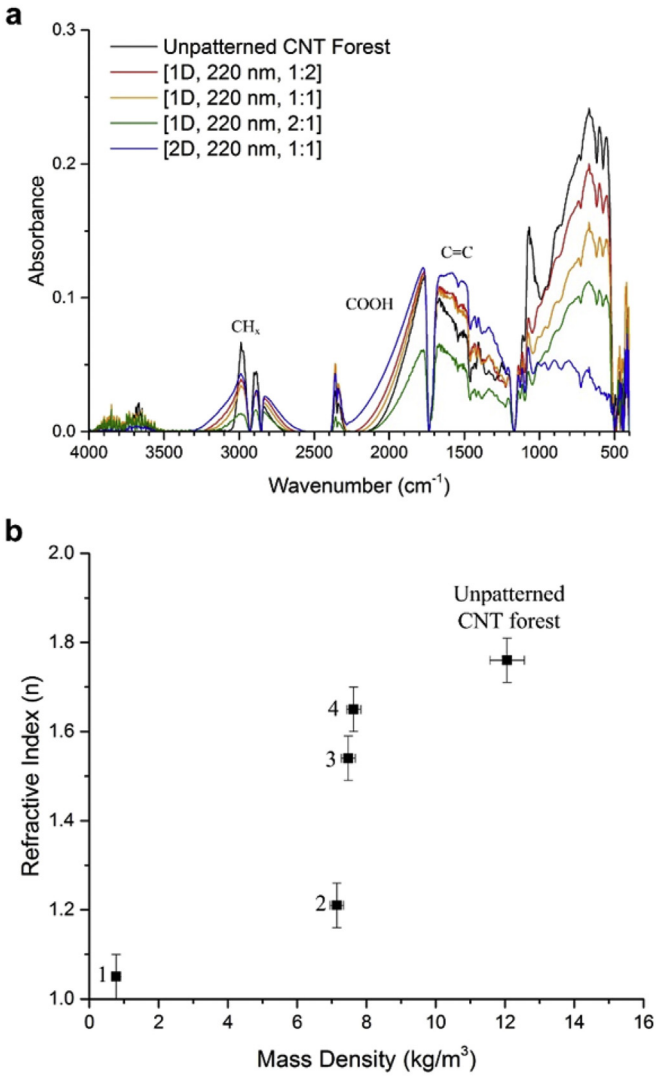

Fig. 5. a) IR absorbance spectra of NIL-patterned CNT forests. Peaks associated with common functional groups are labelled. b) Optical refractive indices (wavenumber 1000 cm^{-1}) of the CNT forests plotted versus mass density. (A colour version of this figure can be viewed online.)

Next, the refractive indices (at wavenumber 1000 cm^{-1}) of the CNT patterns were calculated by performing Kramers-Kronig analysis and are plotted against average mass density (Fig. 5b). The refractive index values range from 1 to 1.8, and are positively correlated with the density. Graphite has a refractive index value of ~4 at this wavenumber [45,46], and by using effective medium theory to approximate CNT forests as air and graphite mixture, it follows that as the density of the CNT forest increases, so will the refractive index. Others have reported that the refractive index linearly increases with decreasing porosity [47]. In our measurements, the relationship was not strictly linear but showed an abrupt increase around 7–8 kg/m^3 (Fig. S3). One possible explanation is that the rough top surface morphology of forests (which is more pronounced at lower mass density, for the more widely spaced patterns) as well as the differences in CNT alignment within the forests would affect the reflection measurements, and hence introduce errors in the refractive index calculations or changes in the effective optical properties.

Interestingly, a small difference in catalyst coverage in the lower coverage regime (25% and 33%) translates to a large difference in the resulting CNT forest mass densities (~1 kg/m^3 and ~7 kg/m^3). This leaves a large gap in the lower density regime (within 1–7 kg/m^3) where the mass densities are presumably very sensitive to the catalyst coverage. The refractive indices of NIL-patterned CNT forests that fall in this range may reveal a different trend, and further add to the ability to tune the refractive index of CNT forests by NIL patterning.

In the case of 1D grating patterns (Patterns 2–6) the grating direction would introduce anisotropy in the samples' optical response. If the incident light has polarization perpendicular to the grating structure, the refractive index would be closer to that of higher density forests, and if the polarization is parallel, it would be closer to that of lower density forests. The variations in different length scales at which the NIL-patterned CNT forests are defined will also influence the optical modulation behavior, especially if the structural length scales become comparable to the wavelength of the incident light such that the light-matter interaction is enhanced. The sub-micrometer features that NIL can impart on the CNT forests provides opportunities to directly tune such interactions.

The demonstrated range of refractive index tuning is from ~1 to ~1.8, which would make the NIL-patterned CNT forests useful for design of gradient index (GRIN) optics. Flat GRIN lenses can be readily designed and produced by laterally varying porosity [48] which could also be achieve by NIL-patterned CNT growth. In addition, the patterns can be designed to incorporate elongated elements with varying orientations, which would make them polarization-selective absorbers that have applications in optical encryption [49], dynamic pixellation [50], polarimetry [51], and single-molecule microscopy [52].

4. Conclusions

Nanoimprint lithography has been successfully used to pattern catalyst films for CNT growth, resulting in modulation of their density and optical refractive index. SEM examination of the top and side surface morphology reveals that the nanoscale patterns translate to CNT nanostructures that grow together to form monolithic structures. The versatility and scalability of the NIL [53,54] is favorable toward fabricating density-graded CNT forests that show directional optical properties of interest. Hierarchical patterning of CNT catalyst may also be achieved by appropriate

design of the mold, and when applied with strain-engineered growth technique [55], or post-growth capillary densification [56], it is expected that density-graded 3D structures can be created.

Conflicts of interest

There are no conflicts of interest to declare.

Acknowledgements

Financial support to S.J.P. and A.J.H. were provided by DARPA (HR0011-10-C-0192). Support from DARPA was received under Agreement to NextGen Aeronautics, and any opinions, findings, and conclusions or recommendations expressed in this material do not necessarily reflect the views of NextGen Aeronautics and/or DARPA. J.G.O. acknowledges the support by the National Research Foundation (NRF) grants funded by the Korean Government Ministry of Science, ICT & Future Planning (MISP) (No. 2015R1A5A1037668 and No. 2016R1C1B2016182) and Samsung Display, Co., Ltd.

Appendix A. Supplementary data

Supplementary data related to this article can be found at https://doi.org/10.1016/j.carbon.2017.11.079.

References

[1] M.M.J. Treacy, T.W. Ebbesen, J.M. Gibson, Exceptionally high Young's modulus observed for individual carbon nanotubes, Nature 381 (6584) (1996) 678–680.
[2] B. Peng, M. Locascio, P. Zapol, S. Li, S.L. Mielke, G.C. Schatz, H.D. Espinosa, Measurements of near-ultimate strength for multiwalled carbon nanotubes and irradiation-induced crosslinking improvements, Nat Nanotechnol. 3 (10) (2008) 626–631.
[3] E. Pop, D. Mann, Q. Wang, K. Goodson, H. Dai, Thermal conductance of an individual single-wall carbon nanotube above room temperature, Nano Lett. 6 (1) (2005) 96–100.
[4] X. Lu, Z. Chen, Curved Pi-conjugation, aromaticity, and the related chemistry of small fullerenes (<C60) and single-walled carbon nanotubes, Chem. Rev. 105 (10) (2005) 3643–3696.
[5] C.Q. Sun, H.L. Bai, B.K. Tay, S. Li, E.Y. Jiang, Dimension, strength, and chemical and thermal stability of a single C–C bond in carbon nanotubes, J. Phys. Chem. B 107 (31) (2003) 7544–7546.
[6] T. Tong, Y. Zhao, L. Delzeit, A. Kashani, M. Meyyappan, A. Majumdar, Dense, vertically aligned multiwalled carbon nanotube arrays as thermal interface materials, Ieee Trans. Compon. Packag. Technol. 30 (1) (2007) 92–100.
[7] T.D.B. Nguyen-Vu, H. Chen, A.M. Cassell, R. Andrews, M. Meyyappan, J. Li, Vertically aligned carbon nanofiber arrays: an advance toward electrical–neural interfaces, Small 2 (1) (2006) 89–94.
[8] Q. Cao, J.A. Rogers, Ultrathin films of single-walled carbon nanotubes for electronics and sensors: a review of fundamental and applied aspects, Adv. Mater. 21 (1) (2009) 29–53.
[9] D.-m. Sun, M.Y. Timmermans, Y. Tian, A.G. Nasibulin, E.I. Kauppinen, S. Kishimoto, T. Mizutani, Y. Ohno, Flexible high-performance carbon nanotube integrated circuits, Nat Nanotechnol. 6 (3) (2011) 156–161.
[10] G.S. Tulevski, A.D. Franklin, D. Frank, J.M. Lobez, Q. Cao, H. Park, A. Afzali, S.-J. Han, J.B. Hannon, W. Haensch, Toward high-performance digital logic Technology with carbon nanotubes, ACS Nano 8 (9) (2014) 8730–8745.
[11] M.M. Shulaker, G. Hills, N. Patil, H. Wei, H.-Y. Chen, H.S.P. Wong, S. Mitra, Carbon nanotube computer, Nature 501 (7468) (2013) 526–530.
[12] J. Meaud, T. Sain, B. Yeom, S.J. Park, A.B. Shoultz, G. Hulbert, Z.-D. Ma, N.A. Kotov, A.J. Hart, E.M. Arruda, A.M. Waas, Simultaneously high stiffness and damping in nanoengineered microtruss composites, Acs Nano 8 (4) (2014) 3468–3475.
[13] Z.-P. Yang, L. Ci, J.A. Bur, S.-Y. Lin, P.M. Ajayan, Experimental observation of an extremely dark material made by a low-density nanotube array, Nano Lett. 8 (2) (2008) 446–451.
[14] K. Mizuno, J. Ishii, H. Kishida, Y. Hayamizu, S. Yasuda, D.N. Futaba, M. Yumura, K. Hata, A black body absorber from vertically aligned single-walled carbon nanotubes, Proc. Natl. Acad. Sci. 106 (15) (2009) 6044–6047.
[15] M. Tarasov, J. Svensson, L. Kuzmin, E.E.B. Campbell, Carbon nanotube bolometers, Appl. Phys. Lett. 90 (16) (2007), 163503.
[16] H. Shi, J.G. Ok, H. Won Baac, L. Jay Guo, Low density carbon nanotube forest as an index-matched and near perfect absorption coating, Appl. Phys. Lett. 99 (21) (2011), 211103.
[17] A.E. Ailev, Y.N. Gartstein, R.H. Baughman, Mirage effect from thermally modulated transparent carbon nanotube sheets, Nanotechnology 22 (43) (2011), 435704.
[18] H. Butt, Q. Dai, R. Rajesekharan, T.D. Wilkinson, G.A.J. Amaratunga, Plasmonic band gaps and waveguide effects in carbon nanotube arrays based metamaterials, ACS Nano 5 (11) (2011) 9138–9143.
[19] L. Ren, C.L. Pint, L.G. Booshehri, W.D. Rice, X. Wang, D.J. Hilton, K. Takeya, I. Kawayama, M. Tonouchi, R.H. Hauge, J. Kono, Carbon nanotube terahertz polarizer, Nano Lett. 9 (7) (2009) 2610–2613.
[20] Y. Tu, Z.P. Huang, D.Z. Wang, J.G. Wen, Z.F. Ren, Growth of aligned carbon nanotubes with controlled site density, Appl. Phys. Lett. 80 (21) (2002) 4018–4020.
[21] X. Liu, T.P. Bigioni, Y. Xu, A.M. Cassell, B.A. Cruden, Vertically aligned dense carbon nanotube growth with diameter control by block copolymer micelle catalyst templates, J. Phys. Chem. B 110 (41) (2006) 20102–20106.
[22] S. Lastella, Y.J. Jung, H. Yang, R. Vajtai, P.M. Ajayan, C.Y. Ryu, D.A. Rider, I. Manners, Density control of single-walled carbon nanotubes using patterned iron nanoparticle catalysts derived from phase-separated thin films of a polyferrocene block copolymer, J. Mater. Chem. 14 (12) (2004) 1791–1794.
[23] Q. Fu, S. Huang, J. Liu, Chemical vapor depositions of single-walled carbon nanotubes catalyzed by uniform Fe_2O_3 nanoclusters synthesized using diblock copolymer micelles, J. Phys. Chem. B 108 (20) (2004) 6124–6129.
[24] J.Q. Lu, T.E. Kopley, N. Moll, D. Roitman, D. Chamberlin, Q. Fu, J. Liu, T.P. Russell, D.A. Rider, I. Manners, High-Quality single-walled carbon nanotubes with small diameter, controlled density, and ordered locations using a polyferrocenylsilane block copolymer catalyst precursor, Chem. Mater. 17 (9) (2005) 2227–2231.
[25] R.D. Bennett, A.J. Hart, R.E. Cohen, Controlling the morphology of carbon nanotube films by varying the areal density of catalyst nanoclusters using block-copolymer micellar thin films, Adv. Mater. 18 (17) (2006) 2274–2279.
[26] L. Delzeit, B. Chen, A. Cassell, R. Stevens, C. Nguyen, M. Meyyappan, Multilayered metal catalysts for controlling the density of single-walled carbon nanotube growth, Chem. Phys. Lett. 348 (5–6) (2001) 368–374.
[27] M. Chhowalla, K.B.K. Teo, C. Ducati, N.L. Rupesinghe, G.A.J. Amaratunga, A.C. Ferrari, D. Roy, J. Robertson, W.I. Milne, Growth process conditions of vertically aligned carbon nanotubes using plasma enhanced chemical vapor deposition, J. Appl. Phys. 90 (10) (2001) 5308–5317.
[28] Y.C. Choi, Y.M. Shin, Y.H. Lee, B.S. Lee, G.-S. Park, W.B. Choi, N.S. Lee, J.M. Kim, Controlling the diameter, growth rate, and density of vertically aligned carbon nanotubes synthesized by microwave plasma-enhanced chemical vapor deposition, Appl. Phys. Lett. 76 (17) (2000) 2367–2369.
[29] L. Zhang, Y. Tan, D.E. Resasco, Controlling the growth of vertically oriented single-walled carbon nanotubes by varying the density of CoMo catalyst particles, Chem. Phys. Lett. 422 (1–3) (2006) 198–203.
[30] G.D. Nessim, A.J. Hart, J.S. Kim, D. Acquaviva, J. Oh, C.D. Morgan, M. Seita, J.S. Leib, C.V. Thompson, Tuning of vertically-aligned carbon nanotube diameter and areal density through catalyst pre-treatment, Nano Lett. 8 (11) (2008) 3587–3593.
[31] J.R. Raney, A. Misra, C. Daraio, Tailoring the microstructure and mechanical properties of arrays of aligned multiwall carbon nanotubes by utilizing different hydrogen concentrations during synthesis, Carbon 49 (11) (2011) 3631–3638.
[32] C. Singh, M.S.P. Shaffer, A.H. Windle, Production of controlled architectures of aligned carbon nanotubes by an injection chemical vapour deposition method, Carbon 41 (2) (2003) 359–368.
[33] F. Wang, M.E. Itkis, E. Bekyarova, R.C. Haddon, Charge-compensated, semiconducting single-walled carbon nanotube thin film as an electrically configurable optical medium, Nat. Photon. 7 (6) (2013) 459–465.
[34] M.-G. Kang, M.-S. Kim, J. Kim, L.J. Guo, Organic solar cells using nanoimprinted transparent metal electrodes, Adv. Mater. 20 (23) (2008) 4408–4413.
[35] J. Li, M. Bedewy, A.O. White, E.S. Polsen, S. Tawfick, A.J. Hart, Highly consistent atmospheric pressure synthesis of carbon nanotube forests by mitigation of moisture transients, J. Phys. Chem. C 120 (20) (2016) 11277–11287.
[36] S.J. Park, A.J. Schmidt, M. Bedewy, A.J. Hart, Measurement of carbon nanotube microstructure relative density by optical attenuation and observation of size-dependent variations, Phys. Chem. Chem. Phys. 15 (27) (2013) 11511–11519.
[37] A.B. Kuzmenko, Kramers–Kronig constrained variational analysis of optical spectra, Rev. Sci. Instrum. 76 (8) (2005), 083108.
[38] M. Bedewy, E.R. Meshot, M.J. Reinker, A.J. Hart, Population growth dynamics of carbon nanotubes, ACS Nano 5 (11) (2011) 8974–8989.
[39] M. Bedewy, A.J. Hart, Mechanical coupling limits the density and quality of self-organized carbon nanotube growth, Nanoscale 5 (7) (2013) 2928–2937.
[40] M.F.L. De Volder, D.O. Vidaud, E.R. Meshot, S. Tawfick, A.J. Hart, Self-similar organization of arrays of individual carbon nanotubes and carbon nanotube micropillars, Microelectron. Eng. 87 (5–8) (2010) 1233–1238.
[41] M. Bedewy, B. Farmer, A.J. Hart, Synergetic chemical coupling controls the uniformity of carbon nanotube microstructure growth, Acs Nano 8 (6) (2014) 5799–5812.
[42] C. Branca, F. Frusteri, V. Magazù, A. Mangione, Characterization of carbon nanotubes by TEM and infrared spectroscopy, J. Phys. Chem. B 108 (11) (2004) 3469–3473.
[43] K. Sbai, A. Rahmani, H. Chadli, J.L. Bantignies, P. Hermet, J.L. Sauvajol, Infrared spectroscopy of single-walled carbon nanotubes, J. Phys. Chem. B 110 (25) (2006) 12388–12393.

[44] N. Kouklin, M. Tzolov, D. Straus, A. Yin, J.M. Xu, Infrared absorption properties of carbon nanotubes synthesized by chemical vapor deposition, Appl. Phys. Lett. 85 (19) (2004) 4463–4465.
[45] P.J. Foster, C.R. Howarth, Optical constants of carbons and coals in the infrared, Carbon 6 (5) (1968) 719–729.
[46] A.B. Djurišić, E.H. Li, Optical properties of graphite, J. Appl. Phys. 85 (10) (1999) 7404–7410.
[47] T.d.l. Arcos, P. Oelhafen, D. Mathys, Optical characterization of alignment and effective refractive index in carbon nanotube films, Nanotechnology 18 (26) (2007), 265706.
[48] S. Ilyas, M. Gal, Gradient refractive index planar microlens in Si using porous silicon, Appl. Phys. Lett. 89 (21) (2006), 211123.
[49] X. Li, T.-H. Lan, C.-H. Tien, M. Gu, Three-dimensional orientation-unlimited polarization encryption by a single optically configured vectorial beam, Nat. Commun. 3 (2012) 998.
[50] H. Yun, S.-Y. Lee, K. Hong, J. Yeom, B. Lee, Plasmonic cavity-apertures as dynamic pixels for the simultaneous control of colour and intensity, Nat. Commun. 6 (2015) 7133.
[51] T. Ellenbogen, K. Seo, K.B. Crozier, Chromatic plasmonic polarizers for active visible color filtering and polarimetry, Nano Lett. 12 (2) (2012) 1026–1031.
[52] M.P. Backlund, A. Arbabi, P.N. Petrov, E. Arbabi, S. Saurabh, A. Faraon, W.E. Moerner, Removing orientation-induced localization biases in single-molecule microscopy using a broadband metasurface mask, Nat. Photon. 10 (7) (2016) 459–462.
[53] J.G. Ok, S.H. Ahn, M.K. Kwak, L.J. Guo, Continuous and high-throughput nanopatterning methodologies based on mechanical deformation, J. Mater. Chem. C 1 (46) (2013) 7681–7691.
[54] J.G. Ok, Y.J. Shin, H.J. Park, L.J. Guo, A step toward next-generation nano-imprint lithography: extending productivity and applicability, Appl. Phys. A 121 (2) (2015) 343–356.
[55] M. De Volder, S. Park, S. Tawfick, A.J. Hart, Strain-engineered manufacturing of freeform carbon nanotube microstructures, Nat. Commun. 5 (4) (2014) 4512.
[56] M. De Volder, S.H. Tawfick, S.J. Park, D. Copic, Z. Zhao, W. Lu, A.J. Hart, Diverse 3D microarchitectures made by capillary forming of carbon nanotubes, Adv. Mater. 22 (39) (2010) 4384–4389.